Biosensors and Bioelectronics 41 (2013) 268–274

Contents lists available at SciVerse ScienceDirect

Biosensors and Bioelectronics

journal homepage: www.elsevier.com/locate/bios

Tubular waveguide evanescent field absorption biosensor based on particle plasmon resonance for multiplex label-free detection

Hsing-Ying Lin [a,1], Chen-Han Huang [a,1], Shin-Huei Chen [b], Yu-Chia Liu [b], Wei-Zhe Chang [b], Lai-Kwan Chau [a,b,c,*]

[a] Center for Nano Bio-Detection, National Chung Cheng University, 168 University Road, Min-Hsiung, Chiayi 621, Taiwan
[b] Department of Chemistry and Biochemistry, National Chung Cheng University, 168 University Road, Min-Hsiung, Chiayi 621, Taiwan
[c] Advanced Institute of Manufacturing with High-tech Innovations, National Chung Cheng University, 168 University Road, Min-Hsiung, Chiayi 621, Taiwan

ARTICLE INFO

Article history:
Received 25 May 2012
Received in revised form
7 August 2012
Accepted 16 August 2012
Available online 29 August 2012

Keywords:
Optical waveguide
Localized surface plasmon resonance
Nanoparticle
Biosensor
High-throughput biochemical detection

ABSTRACT

A novel tubular waveguide particle plasmon resonance (TW-PPR) sensor is demonstrated for label-free biochemical detection. The sensor itself is a microchamber of a defined sample volume, a mechanical support for sensor coating, a waveguide to provide evanescent wave interrogation, and it can be easily extended to a multi-channel format. The sensor resolution is estimated to be 2.6×10^{-6} RIU in measuring solutions of various refractive indices. The sensing system can perform multiple measurements simultaneously and its limit of detection for anti-DNP antibody and streptavidin is 1.2×10^{-10} g/ml (0.55 pM) and 2.3×10^{-10} g/ml (3.5 pM), respectively. Accurate determination of these analytes with known concentration spiked in artificial urine were examined and the bias is less than $\pm7\%$, supporting the utility of the device for analyte screening in more complex media. The TW-PPR sensor can be inexpensively fabricated and has a special niche for monitoring biomolecular interactions in real-time, hence it is ideally suitable for disposable uses, especially promising for convenient high-throughput biochemical sensing applications.

© 2012 Elsevier B.V. All rights reserved.

1. Introduction

Biosensors are powerful detection and analysis tool that has vast applications in biomedical research, healthcare, pharmaceuticals, quality control of food, agriculture, environmental monitoring, and homeland security (Fan et al., 2008; Soper et al., 2006). Surface plasmon resonance (SPR) has attracted considerable research interests for designing biochemical sensors since it can be utilized in highly sensitive real-time and label-free detection (Homola, 2008). The conventional reflectometry configuration of SPR can usually detect refractive index (RI) change of an ambient medium smaller than 10^{-5} (Jung et al., 1998). However, adopting the reflectometry modality somewhat limits the widespread employment of SPR platform.

Measuring the absorbance and spectral shift of localized surface plasmon resonance, also known as particle plasmon resonance (PPR), of noble metal nanoparticles or nanostructures distributed on a substrate via transmission or reflection to interrogate biomolecular interactions, have been demonstrated (Endo et al., 2005; Malinsky et al., 2001; Nath and Chilkoti, 2002; Olofsson et al., 2003; Rauch-Nir et al., 2007). The PPR is the collective oscillation of conduction electrons confined to metal nanoparticles, whose resonance frequency has been shown to be strongly dependent on the particle's size, shape, composition, and the dielectric properties of surrounding medium (Mayer and Hafner, 2011; Stewart et al., 2008). It has been demonstrated that PPR sensor exhibited greater robustness towards interference from bulk RI and higher spatial resolution compared to SPR sensor (Haes and Van Duyne, 2004). Several attractive advantages are provided, such as rapid response time, system simplicity, field portability, and better small molecule sensitivity (Haes and Van Duyne 2004).

Previously, we have successfully combined the PPR properties of gold nanoparticles (AuNPs) with the superiority of high-flux signal transmission of optical fiber to construct a high sensitivity fiber optic sensor, namely FO-PPR sensor (Chau et al., 2006; Cheng and Chau, 2003). The FO-PPR sensor has been applied to biosensing of real samples such as serum (Lai et al., 2007), synovial fluid (Chiang et al., 2010; Hsu et al., 2011), and orchid sample (Chuang et al., 2010). Generally, in fabricating an evanescent wave based fiber optic sensor, a short piece of jacket plus the cladding of fiber need to be removed to render the entry of analyte-containing

* Corresponding author at: Department of Chemistry and Biochemistry, National Chung Cheng University, 168 University Road, Min-Hsiung, Chiayi 621, Taiwan. Tel.: +886 5 2720411; fax: +886 5 2721040x66411.
E-mail address: chelkc@ccu.edu.tw (L.-K. Chau).
[1] These authors contributed equally to this work.

0956-5663/$ - see front matter © 2012 Elsevier B.V. All rights reserved.
http://dx.doi.org/10.1016/j.bios.2012.08.041

sample solution to interact with the evanescent field. For typical silica fibers, once the jacket and cladding are removed, they become fragile and difficult to handle. Therefore, in most evanescent wave based fiber optic sensors, only a few centimeters of the cladding is removed, and this approach limits the sensitivity of fiber optic sensors (Chau et al., 2006; Chiang et al., 2010; Degrandpre and Burgess, 1988). Furthermore, to reduce the response time and sample volume, a customized microfluidic chip must be employed (Hsu et al., 2011).

Up to now, several tubular waveguide sensors consisting of a capillary with a chemically sensitive inner coating have been delivered (Dhadwal et al., 2004; Ligler et al., 2002; Tao et al., 2007; Weigl and Wolfbeis 1994). The optical properties of inner coating vary with the analyte to be measured, and can be interrogated by means of detecting variation of absorption, luminescence, or luminescence lifetime, etc., through evanescent wave spectroscopy. However, to the best of our knowledge, a useful, compact, and possible multi-channel tubular waveguide sensing apparatus has not been reported yet.

This paper presents a tubular waveguide particle plasmon resonance (TW-PPR) sensor, which relies on an unsophisticated light intensity interrogation scheme for biochemical detection. It retains the desirable feature of conventional SPR reflectometry and FO-PPR sensor, the ability to monitor the kinetics of biomolecular interactions in real time without a label, but has one incomparable advantage: the necessity of employing microfluidic chip in the system integration can be circumvented since the tubular waveguide itself is a sample container as well. Importantly, the sensor tubes can be easily arranged into a two-dimensional (2-D) array-based format with the waveguide orthogonal to the plane of array to enable the high-throughput monitoring. Fabricating multiple FO-PPR sensors in a 2-D array format is comparatively tough due to the increased complexity of microfluidic chip design. As compared to the FO-PPR sensor, the inner surface area of TW-PPR sensor tube is much larger than that of the unclad portion of an optical fiber, resulting in the larger quantity of immobilized AuNPs and functionalized bio-probes on the sensing surface, which may give better performance for analyte detection.

Herein, a multi-channel TW-PPR sensing system has been developed (currently seven channels for parallel sample measurement plus one channel for parallel blank measurement). The total detection time for seven samples only takes 12–20 min. The sample injection can be accomplished by using a multi-channel pipette or multiple syringes, which is considered to be particularly convenient for biological samples. The ease and inexpensiveness of TW-PPR sensor make it ideally suitable for disposable uses, and have great potential of being developed into a portable device and applied to point-of-care diagnostics.

2. Materials and methods

2.1. Reagents and materials

Reagents listed in Supplementary Information (S-1) were used as received. All aqueous solutions were prepared with deionized ultrapure water (Milli-Q water purification system, Millipore) with a resistance of 18.2 MΩ cm. Solutions of various RIs ranging from 1.343 to 1.403 were obtained by dissolving sucrose in ultrapure water with a concentration between 6.8% and 41.7% (see supplementary information S-1 for details). Refractive indices of the solutions were measured by a refractometer (Kyoto Electronics, RA-620). Phosphate buffered saline (PBS) solution (pH 7.4) was prepared as containing 150 mM NaCl, 4 mM KCl, 8.1 mM Na_2HPO_4, and 1.47 mM KH_2PO_4. Artificial urine (pH 6.0) was prepared according to the literature (Martinez et al., 2008). Glass tubes (31 mm in length, 5 mm in mouth diameter, 0.4 mm in wall thickness, and 200 μL in volume capacity) were purchased from Grace.

2.2. Fabrication of TW-PPR sensor tubes

Gold nanoparticles employed in our experiments were prepared according to the literature (Cheng and Chau 2003). Glass tubes (see supplementary information, Fig. S1(a)) were cleaned and modified with AuNPs to form a submonolayer with a particle coverage of roughly 24% on the inner wall surface according to the details provided in S-2 (see supplementary information). Absorption spectra of the AuNPs were measured by a Jasco V-570 UV–vis-NIR spectrophotometer. The peak absorbance of AuNPs on the glass tube is typically at 535 nm (see supplementary information, spectrum (I) in Fig. S1(b)). The AuNPs on the surface were taken by a Hitachi 4800I field-emission scanning electron microscope (SEM) operated at 10 kV. The mean diameter of AuNPs determined from the SEM histogram analyses is 15.9 ± 2.6 nm (see supplementary information, Fig. S1(c)). Dinitrophenyl (DNP) group or biotin was functionalized onto the surface of immobilized AuNPs by first forming a self-assembled monolayer (SAM) of cystamine dihydrochloride or a mixed SAM of 11-mercaptoundecanoic acid (MUA) and 6-mercapto-1-hexanol (MCH). Refer to S-3 (see supplementary information) for detailed functionalization procedures and spectral determinations.

2.3. Sensing system and measurements

Effective coupling of light into the tubular inner wall is critical since the working efficiency of plasmonic biosensor depends on the photoexcitation efficiency of the immobilized AuNPs. Here, four mini-LEDs (λ_{ex}=525 nm, dimensions: 0.8 mm × 1.1 mm) were utilized as irradiation source and welded on a self-designed driving circuit board in a circular-shaped arrangement to make them closely meet the mouth diameter of a tube for efficient coupling of light into the tubular waveguide. The transmitted light was then collected at the tube bottom by a photodiode. The central spot of the photodiode is aligned and closely placed at the bottom cone of the tube to record the optical intensity changes. The layout of multi-channel tubular waveguide sensing system is depicted in Fig. 1(a) (refer to supplementary information S-4 for detailed working function of each system component). A picture of multi-channel TW-PPR sensing platform with the footprint smaller than 8 cm × 3 cm which incorporates the optical bench, the TW-PPR sensor tubes, and supporting electronics is presented in the upper section of Fig. 1(b). Each sensor channel is optically isolated from and independent of each other by opaque acrylic plastic, hence, the interference of light scattering and diffraction from adjacent channels can be avoided. To ensure the measurement reproducibility, precise optical alignment of mini-LEDs, tube, and photodiode on the coaxial optical path is required. Moreover, the height of liquid-air interface from channel to channel is kept identical by injection of blanks and samples with equal volume. The lower-left enlarged view in Fig. 1(b) displays the optical waveguide property of ruby-colored TW-PPR sensor tube via the mini-LED excitation. The system setup is less bulky and the configuration allows easier injection and withdrawal of samples and reagents. In addition, as compared with commercial lasers, the mini-LEDs have several attractive advantages, e.g., stable output power, multi-wavelength options, and ease of being integrated into a miniaturized configuration.

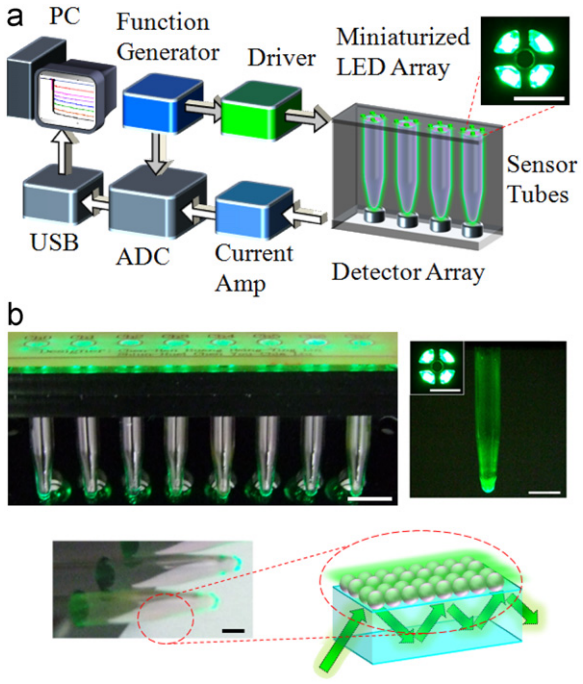

Fig. 1. (a) System layout of multi-channel TW-PPR sensing instrument. Inset: a photograph of circular mini-LED array (scale bar: 5 mm). (b) Upper-left: a picture of multi-channel TW-PPR sensing system (scale bar: 10 mm). Upper-right: a photograph of a single-channel TW-PPR sensor tube irradiated by mini-LEDs (scale bars: 5 mm). The lower-left picture exhibits the waveguide property of a TW-PPR sensor tube (scale bar: 5 mm). The lower-right diagram features the consecutive TIRs and the enhanced evanescent field extensively distributing on the AuNP surface. (For interpretation of the references to color in this figure legend, the reader is referred to the web version of this article.)

3. Results and discussion

3.1. Principle

The sensing technique relies on the penetration of evanescent wave in the absorbing medium of sample solution filled in the sensing chamber and interacting with an analyte (Keller et al., 2007; Wolfbeis 1996). Since light propagates in the tube wall by virtue of consecutive total internal reflections (TIRs), the evanescent field at the inner wall surface excites the PPRs of immobilized AuNPs and thus the light transmitted through the tubular wall is attenuated by interaction with AuNPs. As the attenuation is enhanced by the consecutive TIRs, the low absorbance of a nanoparticle submonolayer can be significantly enhanced by the special niche of large-area and consecutive evanescent field from the waveguide surface (Chau et al., 2006; Degrandpre and Burgess 1988), as displayed in the lower-right schematic diagram of Fig. 1(b). Previous studies (Nath and Chilkoti 2002; Chiang et al., 2010) have shown that the bulk absorption coefficient of AuNP layer increases when the AuNP's surrounding RI increases. Hence, the increase of local RI at the AuNP surface after molecular binding can be revealed by a decrease of transmitted light intensity through the tube. In this study, the quantitative analyses of evanescent wave absorption measurements of TW-PPR sensor are performed by comparing the collected optical signal of a sensor immersed in an analyte solution (I_S) to the intensity of the sensor immersed in a blank solution (I_0). The sensor response is defined as I_S/I_0.

Two parameters, sensor sensitivity and sensor resolution, are used to characterize the sensor performances. The sensor sensitivity to RI change is the slope of the plot of sensor response versus RI (Huang et al., 2012). The sensor resolution is defined as the minimum change in refractive index unit (RIU) that can be resolved by the sensor, where the noise is taken as the standard deviation of the sensor response for 10 repetitive measurements of a blank (Hsu et al., 2011).

3.2. Single-channel TW-PPR sensing platform

To quantify the sensor responses of a single-channel TW-PPR sensor to bulk RI variations, solutions of increasing sucrose concentration with known RIs were successively injected in and drawn out the sensing channel while the transmitted optical signal was synchronously recorded. The corresponding sensorgram is illustrated in Fig. 2(a), where the signal intensity is normalized to the baseline intensity. The baseline was established as the TW-PPR sensor was filled with a defined amount of ultrapure water. With the step-wise increase of RI, the signal intensity shows a step-down trend, resulting from the increased evanescent field absorption by the immobilized AuNPs at higher surrounding RI. The measurement of signal intensity under multi-step RI changes was repeated ten times sequentially by using ten different sensor tubes. The corresponding calibration curve plus error bars are shown in Fig. 2(b). The power stability is estimated to be $\pm 0.0027\%$ per 2000 s. The sensor resolution of the sensor is approximately 2.62×10^{-6} RIU, which is comparable to the value

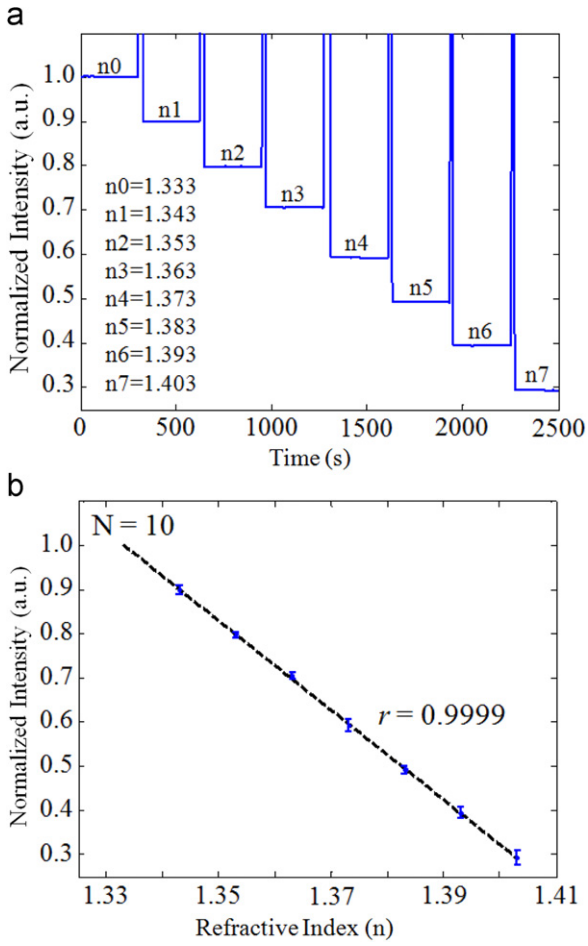

Fig. 2. (a) Real-time TW-PPR sensor responses during the sequential introduction of various RI solutions prepared by different concentration of sucrose in ultrapure water. The RIs of step 0–7 are shown in the graph. (b) The corresponding calibration curve depicts the linear regression between the sample RI and the normalized optical signal intensity. Error bars are derived from ten repetitive measurements. The correlation coefficient of the linear plot is estimated to be 0.9999.

of 1.9×10^{-6} RIU demonstrated by the FO-PPR sensor (Hsu et al., 2011). The calculated correlation coefficient (r) is 0.9999, indicating a good linear relationship between signal intensity and RI over the RI range of 1.333 to 1.403.

As a proof-of-concept to demonstrate that such a compact setup can be applied to real-time biochemical detection, model experiments in buffer to kinetically monitor molecular recognition events were carried out. Prior to these biochemical measurements, nonspecific adsorption tests were performed to verify the results. For DNP- and biotin-functionalized TW-PPR sensors, both the sensor responses in the presence of 10^{-5} g/ml bovine serum albumin (BSA, Sigma) were indistinguishable from the background signal (see supplementary information, Fig. S2 and S3). These results indicate that there was negligible nonspecific adsorption from high concentration of BSA. Refractive indices of PBS, BSA, anti-DNP antibody, and streptavidin solutions were measured by the refractometer. There is no significant RI difference between the blank and the analyte solutions. Therefore, we can make sure that the measured signal change was caused by the specific binding event between analyte and corresponding recognition molecules on the AuNP surface.

Hereafter, both DNP- and biotin-functionalized TW-PPR sensors were employed to detect anti-DNP antibody and streptavidin spiked in buffer, respectively, by serial injection of increasing concentration of the corresponding targets. As shown in Fig. 3(a), the transmitted optical intensity in the steady-state decreases with the increasing concentration of streptavidin. Here, the limit of detection (LOD) is defined as the sensor response (I_S/I_0) that yields a signal-to-noise ratio of 3, where the noise is taken as the standard deviation of I_S/I_0 for 10 repetitive measurements in buffer. From the calibration graph as shown in Fig. 3(b), a LOD of 2.3×10^{-10} g/ml (3.4 pM) for streptavidin is estimated. In comparison with the LOD of 1.7×10^{-8} M determined by biotin-functionalized AuNPs on a glass slide via a single-pass transmission mode, the LOD value of TW-PPR sensor is much lower and is significantly improved by up to 3.7-order (Olofsson et al., 2003). Similarly, a LOD of 1.2×10^{-10} g/ml (0.52 pM) for anti-DNP antibody is estimated (see supplementary information, Fig. S4). These values are lower than those of the FO-PPR sensor being encapsulated in a microfluidic flow-cell, which have LODs of 11 pM and 1.2 pM for streptavidin and anti-DNP antibody, respectively. The improvement of LOD is considered to be attributed to the large-area and hence larger number of immobilized AuNPs which accommodate a larger quantity of bio-probes functionalized on the waveguide surface for analyte detection.

3.3. Multi-channel TW-PPR sensing platform

The sensor resolution of the multi-channel TW-PPR sensing platform was also evaluated. Fig. 4(a) exhibits the sensorgrams of simultaneous sensor responses from the multi-channel sensing platform, for which the reference channel (Ch0) was filled with a defined volume of ultrapure water and each detection channel (Ch1–Ch7) was filled with a defined volume of water first, then removed, and refilled with a sucrose solution with the same defined volume and a known RI value, while the RI values of the sucrose solutions in each detection channel are different.

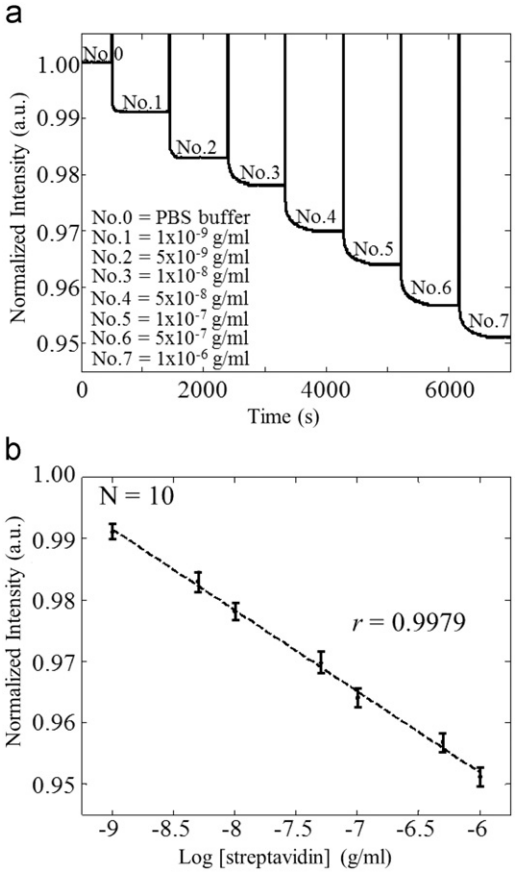

Fig. 3. (a) Typical sensor responses to different concentrations of streptavidin solution using single-channel biotin-functionalized TW-PPR sensing platform. (b) Calibration curve for normalized optical intensity in response to various concentrations of streptavidin solution. The correlation coefficient of the linear plot is estimated to be 0.9979

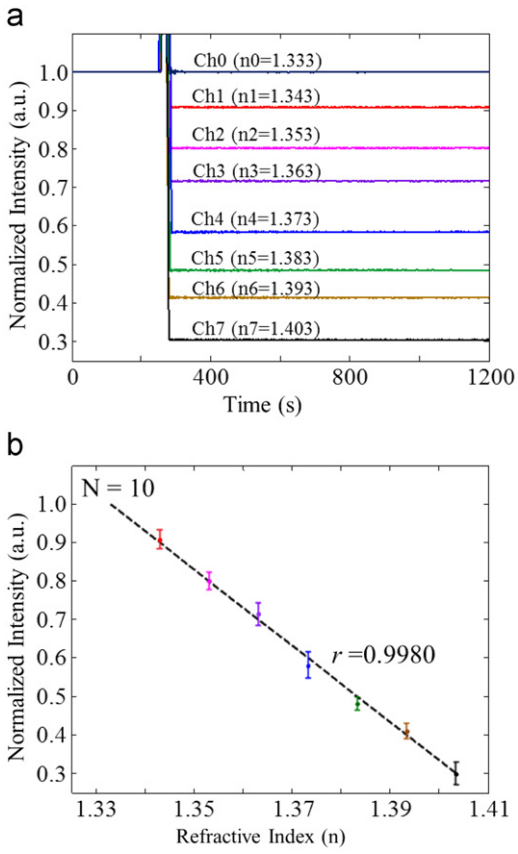

Fig. 4. (a) Temporal sensor responses of multi-channel TW-PPR sensing system, in which each channel was injected with a solution of sucrose of defined RI. (b) The calibration plot of multi-channel TW-PPR sensing platform by parallel measurements of sucrose solutions and a correlation coefficient of 0.9980 is estimated. Error bars are obtained from ten repetitive measurements.

The sensor response of each sensor tube filled with ultrapure water was used to establish a baseline. For which, a flat baseline is essential to ensure the optical stability of the system. In this regard, the reference channel is used to monitor the stability of the baseline during the course of binding reactions in the detection channels and can provide a possibility to compensate the environmental fluctuations. The resultant RI calibration curve is shown in Fig. 4(b). A highly linear regression of the signal intensity with RI change can be obtained with r of 0.9980. Error bars are derived from ten repetitive simultaneous measurements. By the calibration curve, the sensor resolution of the multi-channel TW-PPR sensing platform is estimated to be 2.64×10^{-6} RIU. This value is barely higher than that of the single-channel TW-PPR sensing platform presented in Fig. 2(b), and the very small difference is supposed to be attributed to inherent systematic deviations from channel-to-channel and tube-to-tube.

As a proof-of-concept to demonstrate that the multi-channel TW-PPR sensing platform can be applied to the detection of multiple biological samples in parallel, we carried out model experiments in buffer to simultaneously monitor the kinetic binding events. Both DNP- and biotin-functionalized TW-PPR sensors were employed to detect anti-DNP antibody and streptavidin, respectively, by injection of corresponding targets with various concentrations into different tubes. Similar to the above experiments for determination of sensor resolution, the same protocol was used except that a buffer instead of ultrapure water was employed to establish a baseline. The sensorgrams of the temporal multi-channel sensor responses to various concentrations of anti-DNP antibody ranging from 10^{-9} g/ml to 10^{-6} g/ml is depicted in Fig. 5(a). The transmitted optical intensity decreased with increasing concentration of anti-DNP antibody. The corresponding calibration curve is plotted in Fig. 5(b). Error bars represent standard deviations from ten repetitive measurements using different tubes. The coefficients of variations (CVs) of the sensor responses at the seven different concentrations are between 3.96% and 9.83%, suggesting the performance of the sensor tubes is reasonably reproducible. From the calibration curve, a linear fit with r of 0.9975 between the normalized optical intensity and the logarithmic concentration of anti-DNP antibody is obtained and a LOD of 1.2×10^{-10} g/ml (0.55 pM) is obtained. Similarly, a LOD of 2.3×10^{-10} g/ml (3.5 pM) for streptavidin is estimated (see supplementary information, Fig. S5). These values are close to those of the single-channel TW-PPR sensing platform presented in Figs. 3(b) and S4(b) (see supplementary information).

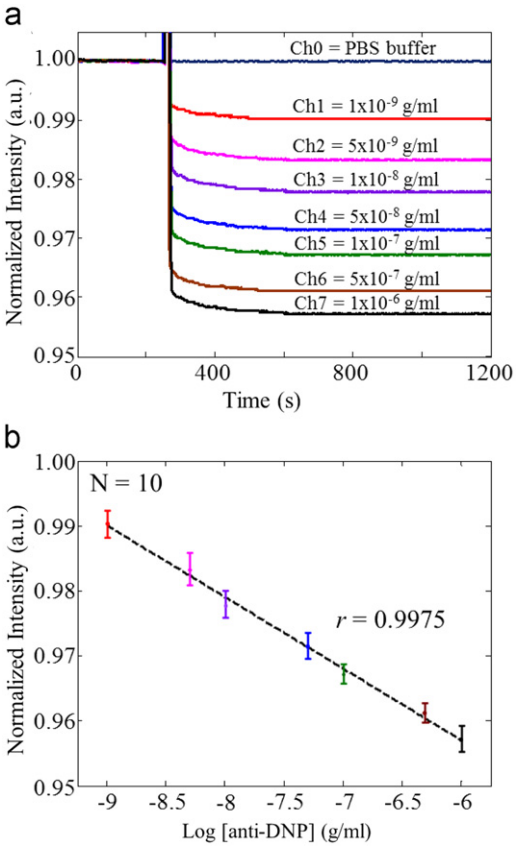

Fig. 5. (a) Temporal sensor responses of multi-channel DNP-functionalized TW-PPR sensing system to different concentrations of anti-DNP antibody spiked in PBS solution. (b) The corresponding calibration graph of ten repetitive measurements of different concentrations of anti-DNP antibody in correlation with normalized optical intensity. The correlation coefficient is 0.9975. (For interpretation of the references to color in this figure legend, the reader is referred to the web version of this article.)

3.4. Evaluation of affinity constant

The affinity constant (also known as the association constant), K_a, is a widely used parameter applied to characterize the binding strength between two interacting molecules at equilibrium. The functionalization of molecules onto a surface may alter the binding characteristics of the system, and thus the characteristics of immobilized molecular probes and their effect on the binding dynamics has to be assessed. From Langmuir adsorption model and equations provided in S-6 (see supplementary information), K_a can be calculated from the ratio between the intercept and slope of a linear plot of $1/(I_0-I_S)$ against $1/[x]_0$. The linear fits give $K_a = 9.3 \times 10^8\ M^{-1}$ and $6.5 \times 10^8\ M^{-1}$, respectively for DNP–anti-DNP antibody and biotin–streptavidin complexes. The derived K_a value of DNP–anti-DNP antibody complex is comparable to that determined by fluorescence spectroscopy in solution ($1.25 \times 10^9\ M^{-1}$) (Bilgicer et al., 2007) and that by FO-PPR sensor ($4.8 \times 10^8\ M^{-1}$) (Chau et al., 2012) and quartz crystal microbalance ($2.2 \times 10^8\ M^{-1}$) (Senaratne et al., 2006). Moreover, the K_a value of biotin–streptavidin complex is comparable to that determined by SPR sensor (1.8×10^8–$3.0 \times 10^8\ M^{-1}$) (Ke et al., 2007). As such, the results indicate that a probe-functionalized TW-PPR sensor is able to convert the information of a molecular probe-analyte recognition event into a detectable optical intensity change that is useful to assess biomolecular interactions.

3.5. Quantitative measurement of analytes in artificial urine

It is essential for a desirable sensing system to possess the capability of direct determination of specific analytes in the physiological environment for rapid medical and clinical diagnosis. Herein, the artificial urine was used as a representative biological fluid since it is the most informative physiological fluid that can be obtained noninvasively. To validate the potential of the TW-PPR sensing system to be applied to real samples, we performed parallel detection of sample solutions with known concentration of anti-DNP antibody or streptavidin in artificial urine by using DNP- or biotin-functionalized sensor tubes, respectively. The PBS was used as a diluent as well as a blank solution. Urine solutions spiked with anti-DNP antibody or streptavidin at concentrations of 10^{-5} g/ml, 10^{-6} g/ml, and 10^{-7} g/ml were diluted 20-fold before the assay. The extent of dilution relies on the fact that the measured RI (n=1.33436) of diluted sample solutions shows no significant RI difference from the measured RI (n=1.33436) of the buffer. The buffer solution was first injected into each of the sensing channels and then removed. Among these channels, one channel was employed as a

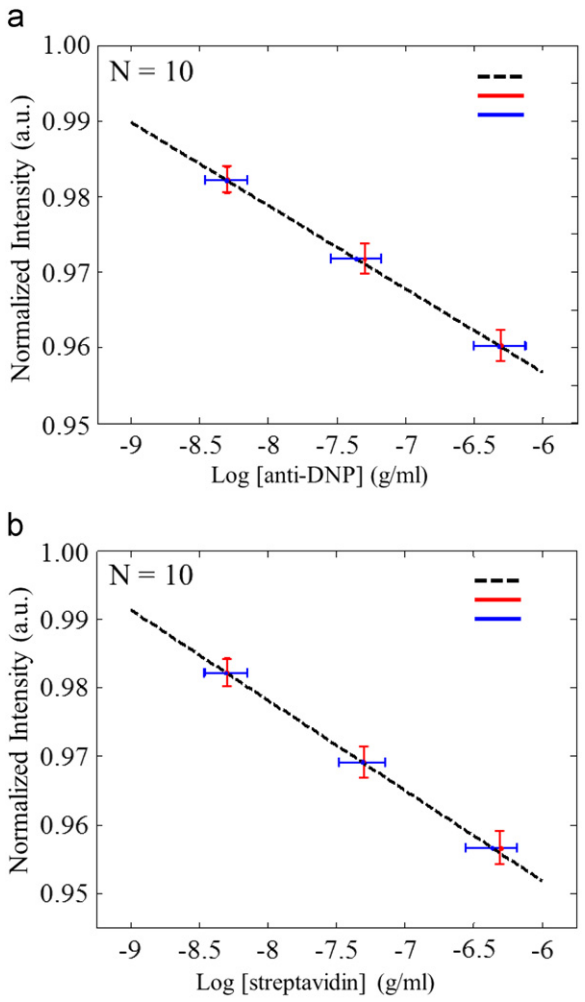

Fig. 6. Quantitative detection of different concentrations of (a) anti-DNP antibody or (b) streptavidin spiked in artificial urine using DNP- or biotin-functionalized TW-PPR sensor tubes, respectively. Red vertical error bars are derived from ten repetitive measurements. Calibration curves in (a) and (b) represented by black dash lines are obtained from standard calibration curves described respectively in Fig. 5(b) and S5 (b). Blue horizontal error bars exhibit the measured concentration range of analyte obtained by introducing the values of red vertical error bars into the standard calibration curve. (For interpretation of the references to color in this figure legend, the reader is referred to the web version of this article.)

reference channel with only buffer injected and the others were used as detection channels with sample injected after the buffer solutions were withdrawn. Subsequently, diluted urine samples with anti-DNP antibody or streptavidin concentrations of 5×10^{-7} g/ml, 5×10^{-8} g/ml, and 5×10^{-9} g/ml were simultaneously analyzed by the probe-functionalized TW-PPR sensor array. Fig. 6 illustrates the plots of normalized intensity of signal versus the analyte concentration. The CVs of the sensor responses from high to low concentrations of anti-DNP antibody and streptavidin detections depicted by red vertical error bars is obtained from ten repetitive measurements using ten different sensor tubes and is found to be 5.28%, 7.08%, and 9.54% for anti-DNP antibody, and 5.56%, 7.14%, and 11.30% for streptavidin, respectively. The calculated concentration of analyte was obtained by introducing the measured signal into the standard calibration curve of model experiments shown in Figs. 5(b) and S5(b) (see supplementary information). The bias of the analysis is in the range of −5.3–6.1% and −6.8–5.1%, respectively for anti-DNP antibody and streptavidin (see supplementary information, Table S1). Blue horizontal error bars exhibit the uncertainty of the measured concentration range of analyte obtained by introducing the values of red vertical error bars into the standard calibration curve. From the analytical comparison plots, it is seen that the data points are distributed along the regression line of the standard calibration curves, thus indicating that the artificial urine matrix does not interfere with the specific detection of anti-DNP antibody and streptavidin using this sensing platform. This demonstrates the potential of the TW-PPR sensing platform for quantitative detection of a specific analyte in a complex sample medium such as urine if the standard calibration curve of the analyte is pre-determined.

4. Conclusion

The feasibility of single- and multi-channel biochemical detection by using probe-functionalized TW-PPR sensor based on optical intensity interrogation scheme is demonstrated. The detection sensitivity of both single- and multi-channel TW-PPR sensing systems is comparable with that of an alternative waveguide-based PPR sensor, the FO-PPR sensor. The TW-PPR sensor offers significant improvements with respect to system simplicity and operation convenience. It can provide quantitative detection of analyte in both buffer and artificial urine, and can be used to characterize the probe–analyte molecular interaction, including the evaluation of K_a constant. Extra benefits are short assay time and cost-effective. These proof-of-concept findings together suggest that the disposable TW-PPR sensor associated with multi-channel sensing platform can be employed for high-throughput and parallelized analysis of biochemical reactions, and make it a viable alternative to other more costly or bulky well-established analytical tools for biochemical research and analysis.

Acknowledgements

Gratefully acknowledge the financial support from National Science Council of Taiwan (NSC100-2120-M-194-005-CC1).

Appendix A. Supporting information

Supplementary data associated with this article can be found in the online version at http://dx.doi.org/10.1016/j.bios.2012.08.041.

References

Bilgicer, B., Moustakas, D.T., Whitesides, G.M., 2007. Journal of the American Chemical Society 129, 3722–3728.
Chau, L.-K., Chiang, C.-Y., Hsu, W.-T., Chen, S.-H., Cheng, S.F., 2012. Optical waveguide-based biosensors using noble metal nanoparticles. In: Chau, L.-K., Chang, H.-T. (Eds.), From Bioimaging to Biosensors: Noble Metal Nanoparticles in Biodetection. Pan Stanford Publishing, Singapore, pp. 77–102 (Chapter 5).
Chau, L.-K., Lin, Y.-F., Cheng, S.-F., Lin, T.-J., 2006. Sensors and Actuators B 113, 100–105.
Cheng, S.F., Chau, L.K., 2003. Analytical Chemistry 75, 16–21.
Chiang, C.-Y., Hsieh, M.-L., Huang, K.-W., Chau, L.-K., Chang, C.-M., Lyu, S.-R., 2010. Biosensors and Bioelectronics 26, 1036–1042.
Chuang, Y., Lee, C.Y., Lu, S.H., Wang, S.C., Chau, L.K., Hsieh, W.H., 2010. Analytical Chemistry 82, 1123–1127.
Degrandpre, M.D., Burgess, L.W., 1988. Analytical Chemistry 60, 2582–2586.
Dhadwal, H.S., Kemp, P., Aller, J., Dantzler, M.M., 2004. Analytica Chimica Acta 501, 205–217.
Endo, T., Yamamura, S., Nagatani, N., Morita, Y., Takamura, Y., Tamiya, E., 2005. Science and Technology of Advanced Materials 6, 491–500.
Fan, X.D., White, I.M., Shopova, S.I., Zhu, H.Y., Suter, J.D., Sun, Y.Z., 2008. Analytica Chimica Acta 620, 8–26.
Haes, A.J., Van Duyne, R.P., 2004. Analytical and Bioanalytical Chemistry 379, 920–930.
Homola, J., 2008. Chemical Reviews 108, 462–493.
Hsu, W.T., Hsieh, W.H., Cheng, S.F., Jen, C.P., Wu, C.C., Li, C.H., Lee, C.Y., Li, W.Y., Chau, L.K., Chiang, C.Y., Lyu, S.R., 2011. Analytica Chimica Acta 697, 75–82.

Huang, K.-W., Hsieh, C.-W., Kan, H.-C., Hsieh, M.-L., Hsieh, S., Chau, L.-K., Cheng, T.-E., Lin, W.-T., 2012. Sensors and Actuators B 163, 207–215.
Jung, L.S., Campbell, C.T., Chinowsky, T.M., Mar, M.N., Yee, S.S., 1998. Langmuir 14, 5636–5648.
Ke, S., Wright, J.C., Kwon, G.S., 2007. Bioconjugate Chemistry 18, 2109–2114.
Keller, B.K., DeGrandpre, M.D., Palmer, C.P., 2007. Sensors and Actuators B 125, 360–371.
Lai, N.-S., Wang, C.-C., Chiang, H.-L., Chau, L.-K., 2007. Analytical and Bioanalytical Chemistry 388, 901–907.
Ligler, F.S., Breimer, M., Golden, J.P., Nivens, D.A., Dodson, J.P., Green, T.M., Haders, D.P., Sadik, O.A., 2002. Analytical Chemistry 74, 713–719.
Malinsky, M.D., Kelly, K.L., Schatz, G.C., Van Duyne, R.P., 2001. Journal of the American Chemical Society 123, 1471–1482.
Martinez, A.W., Phillips, S.T., Carrilho, E., Thomas, S.W., Sindi, H., Whitesides, G.M., 2008. Analytical Chemistry 80, 3699–3707.
Mayer, K.M., Hafner, J.H., 2011. Chemical Reviews 111, 3828–3857.
Nath, N., Chilkoti, A., 2002. Analytical Chemistry 74, 504–509.
Olofsson, L., Rindzevicius, T., Pfeiffer, I., Käll, M., Höök, F., 2003. Langmuir 19, 10414–10419.
Rauch-Nir, I., Bendikov, T.A., Doron-Mor, I., Barkay, Z., Vaskevich, A., Rubinstein, I., 2007. Journal of the American Chemical Society 129, 84–92.
Senaratne, W., Takada, K., Das, R., Cohen, J., Baird, B., Abruña, H.D., Ober, C.K., 2006. Biosensors and Bioelectronics 22, 63–70.
Soper, S.A., Brown, K., Ellington, A., Frazier, B., Garcia-Manero, G., Gau, V., Gutman, S.I., Hayes, D.F., Korte, B., Landers, J.L., Larson, D., Ligler, F., Majumdar, A., Mascini, M., Nolte, D., Rosenzweig, Z., Wang, J., Wilson, D., 2006. Biosensors and Bioelectronics 21, 1932–1942.
Stewart, M.E., Anderton, C.R., Thompson, L.B., Maria, J., Gray, S.K., Rogers, J.A., Nuzzo, R.G., 2008. Chemical Reviews 108, 494–521.
Tao, S.Q., Gong, S.D., Fanguy, J.C., Hu, X.M., 2007. Sensors and Actuators B 120, 724–731.
Weigl, B.H., Wolfbeis, O.S., 1994. Analytical Chemistry 66, 3323–3327.
Wolfbeis, O.S., 1996. TrAC Trends in Analytical Chemistry 15, 225–232.